

Bond graph modelling and simulation of fault scenarios in switched power electronic systems

Wolfgang Borutzky

Proc IMechE Part I:
J Systems and Control Engineering
226(10) 1381–1393
© IMechE 2012
Reprints and permissions:
sagepub.co.uk/journalsPermissions.nav
DOI: 10.1177/0959651812454636
pii.sagepub.com


Abstract

A bond graph representation of switching devices known for a long time has been a modulated transformer with a modulus $b(t) \in \{0, 1\} \forall t \geq 0$ in conjunction with a resistor $R : R_{on}$ accounting for the ON-resistance of a switch considered non-ideal. Besides other representations, this simple model has been used in bond graphs for simulation of the dynamic behaviour of hybrid systems. A previous article of the author has proposed to use the transformer–resistor pair in bond graphs for fault diagnosis in hybrid systems. Advantages are a unique bond graph for all system modes, the application of the unmodified standard Sequential Causality Assignment Procedure, fixed computational causalities and the derivation of analytical redundancy relations incorporating ‘Boolean’ transformer moduli so that they hold for all system modes. Switches temporarily connect and disconnect model parts. As a result, some independent storage elements may temporarily become dependent, so that the number of state variables is not time-invariant. This article addresses this problem in the context of modelling and simulation of fault scenarios in hybrid systems. In order to keep time-invariant preferred integral causality at storage ports, residual sinks previously introduced by the author are used. When two storage elements become dependent at a switching time instance t_s , a residual sink is activated. It enforces that the outputs of two dependent storage elements become immediately equal by imposing the conjugate power variable of appropriate value on their inputs. The approach is illustrated by the bond graph modelling and simulation of some fault scenarios in a standard three-phase switched power inverter supplying power into an RL -load in a delta configuration. A well-developed approach to model-based fault detection and isolation is to evaluate the residual of analytical redundancy relations. In this article, analytical redundancy relation residuals have been computed numerically by coupling a bond graph of the faulty system to one of the non-faulty systems by means of residual sinks. The presented approach is not confined to power electronic systems but can be used for hybrid systems in other domains as well. In further work, the RL -load may be replaced by a bond graph model of an alternating current motor in order to study the effect of switch failures in the power inverter on to the dynamic behaviour of the motor.

Keywords

Hybrid systems, system mode independent bond graph representation, fault scenarios, residual sinks, fault detection and isolation, analytical redundancy relation residuals, switched three-phase power inverter

Date received: 14 April 2012; accepted: 22 June 2012

Hybrid system models

In the modelling of various engineering systems such as power electronic systems, devices such as check valves in hydraulic systems, clutches or physical effects such as stick–slip effects and stops in mechanical motion, it is convenient and common to neglect the short time intervals in which fast transitions from one system mode to another take place and to use the abstraction that the change of state happens instantaneously either controlled or autonomously. This abstraction of discrete time events can be justified because the continuous time dynamics of fast state

transitions during short time intervals is not of relevance for the overall dynamic behaviour of a system. Hybrid system models encompass dynamic continuous time system behaviour as well as discrete time, discontinuous events. The abstraction of instantaneous discontinuous state transitions entails that:

Bonn-Rhein-Sieg University of Applied Sciences, Germany

Corresponding author:

Wolfgang Borutzky, Bonn-Rhein-Sieg University of Applied Sciences, Sankt Augustin, D-53754 Germany.
Email: wolfgang.borutzky@h-brs.de

model parts are temporarily disconnected and reconnected, namely, the model structure becomes system mode dependent;
 storage elements may become temporarily dependent, so that the number of state variables is not time-invariant;
 the time instances of discrete events must be determined during simulation;
 numerical integration of ordinary differential equations (ODEs) may need to be reset at the advent of a discrete event.

As to simulation, numerical mathematics has contributed differential algebraic equation (DAE) solvers that enable to automatically locate the time instances of discrete events and to restart the numerical integration with proper initial values.

Bond graph representations of hybrid system models

As bond graph (BG) modelling starts from considering the exchange of energy between system components and processes, being time continuous, BGs were initially confined to the representation of continuous time models. Causal BGs were mainly developed to have a software program derive a set of ODEs or DAEs in order to simulate the dynamic behaviour of a system. In addition, for a long time, BG representations of hybrid system models have also been considered, and various approaches have been reported in the literature (see, for instance, Borutzky^{1,2}).

An early proposal has been made to represent fast switching elements by means of a modulated transformer (MTF) controlled by a variable $b(t) \in \{0, 1\} \forall t \geq 0$ (i.e. MTF : b). Depending on the value of the transformer modulus, model parts linked by such MTFs are either connected or disconnected. Furthermore, in power electronics, it has been proposed to approximate the constitutive characteristic of devices such as diodes or thyristors by a piecewise linear function that accounts for the ON-resistance (cf. Figure 1).

Accordingly, switches have been modelled by means of a transformer modulated by a variable $b(t) \in \{0, 1\} \forall t \geq 0$ in conjunction with a resistor $R : R_{on}$ in fixed conductance causality accounting for a small resistance in ON-mode³⁻⁵ (cf. Figure 5). More recently, Umarikar introduced so-called switched power junctions (SPJs).⁶ They may have more than one bond determining causalities at their ports, but only one of these bonds is activated at a time by a signal controlling the junction.

Other approaches to capture the abstraction of instantaneous state switches in a BG have been the natural introduction of the ideal switch as another BG element⁷⁻¹⁰ or the introduction of junctions that are controlled by a local automaton.^{11,12} For BGs with controlled junctions, the notion *hybrid* bond graph (HBG)

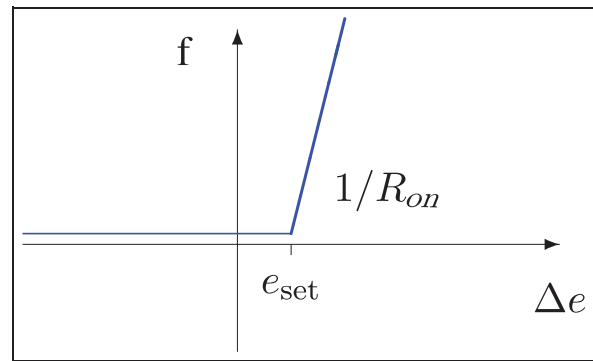


Figure 1. Piecewise linear characteristic of a switching element accounting for the ON-resistance.

is used in the literature. In BGs using the ideal switch as another BG element or using controlled junctions, computational causalities are no longer time-invariant but become dependent on switch states. For n switches in a model, there are $m \leq 2^n$ physically feasible switch state combinations. Each one constitutes a system mode. Theoretically, these system modes and their corresponding causal BG model accounting for the dynamic behaviour in that system mode can be determined prior to simulation. During simulation, computation can switch from the causal BG model of a current system mode to the model valid for the next system mode.

In a bond graph-based approach to fault detection and isolation (FDI) in hybrid system models, the author has used the above MTF- R pair for modelling switching devices.¹ The advantages are that:

- a unique BG can be set up that holds for all system modes;
- the standard Sequential Causality Assignment Procedure (SCAP) can be applied without modification resulting in fixed computational causalities;
- a single set of model equations as well as equations for fault indicators valid for all system modes can be (automatically) derived from the BG.

Clearly, fault indicators should be sensitive to true faults but robust to parameter uncertainties in order to avoid missing faults or reporting false alarms to a process supervision system. In Borutzky,¹³ the author has shown that by coupling a BG to an *incremental* BG (Chapter 4 of Borutzky¹⁴), thresholds for fault indicators in hybrid system models can be obtained, which adapt to system modes and enable robust FDI with regard to parameter uncertainties. Another approach has been the use of BGs in the so-called linear transformation form (LTF) for the same purpose (see, for instance, Chapter 3 of Borutzky¹⁴).

Residual sinks

Changing switch states in hybrid system models may entail that the number of state variables of a hybrid system model is not a static invariant but may change

from one system mode to another. This means that in a BG representation of a hybrid model, causality at some storage ports may change from integral to derivative causality. Preferred integral causality may be preserved by using artificial so-called residual sinks introduced by the author.¹⁵ Depending on its type, a residual sink imposes either an effort or a flow on two dependent storage elements, so that their output variables become equal. As a result, the underlying mathematical models become a DAE system because there is no ODE for the outputs of the residual sinks but algebraic constraints for the output variables of some storage elements.

In a hybrid system BG, residual sinks must be activated whenever a system mode change happens and causes two storage elements to become dependent. This can be achieved by a ‘Boolean’ controlled transformer as depicted in the BG fragment of Figure 2. As to the numerical computation of the dynamic behaviour, this means that numerical integration must be re-initialised at the switching time instant when the residual sink is activated. The outputs of two storage elements becoming dependent jump to a common value, and integration restarts from this value.

In the following, the approach to BG model-based FDI of hybrid systems proposed in Borutzky¹ is extended by combining it with the use of residual sinks accounting for a system mode-dependent number of state variables and allowing for keeping fixed preferred integral causality. This extended approach is illustrated by a case study considering various fault scenarios in a switching three-phase power inverter supplying power to a delta *RL*-load.

Switched three-phase power inverter

Figure 3 shows a circuit schematic of a switched three-phase power inverter that supplies power to a

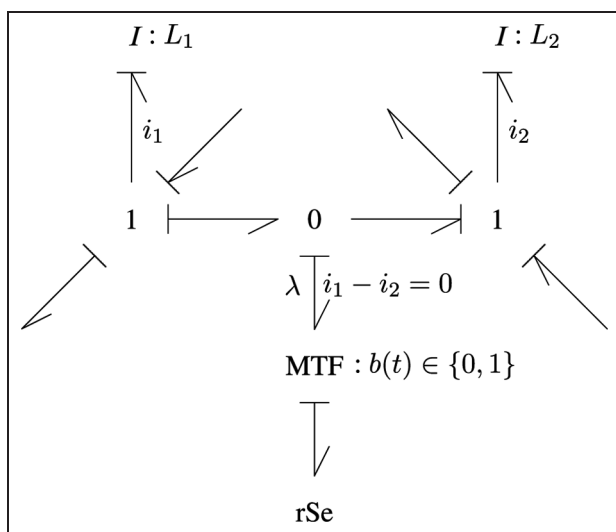


Figure 2. Residual effort sink rSe enforcing a common flow for two *l*-storage elements.

three-phase *RL*-load in a delta configuration. The control voltages U_i at the transistor bases B_i ($i = 1, \dots, 6$) are provided according to a six-step inverter modulation policy. Control signals U_1, U_2 and U_3 are sinusoidal waveforms with negative values set to zero and positive values set to one and with a phase displacement of 120° between them. The remaining control signals are $U_4 = 1 - U_1, U_5 = 1 - U_2$ and $U_6 = 1 - U_3$, respectively.

In Junco et al.¹⁶ and in Chapter 8 of Borutzky,¹⁴ Junco et al. use this power electronic system as an example for the application of their implementation of the non-standard SPJs⁶ in the modelling language of the 20-sim software.¹⁷ In their model used for simulating the dynamic behaviour of the healthy system, they represent the transistor–diode pair in each inverter half-bridge by means of an SPJ assuming this pair can be considered an ideal switch.

Bond graph model of the power inverter

In this article, the transistor–diode pairs are modelled as non-ideal switches with an ON-resistance R_{on} . Their BG representation is an MTF : *m* with a modulus $m(t) \in \{0, 1\} \forall t \geq 0$ in conjunction with a resistor $R : R_{on}$. Figures 4 and 5 show a BG of the three-phase inverter. Computational causalities in this BG are fixed for all system modes due to the fixed conductance causality of the switch resistors. The three half-bridges of the inverter are indexed as *a*, *b* and *c*, respectively. Furthermore, an index *p* relates to the upper switch of a half-bridge, while an index *n* indicates the lower switch. Accordingly, $m_{ap}(t)$ denotes the transformer modulus of the upper switch in the half-bridge with the index ‘*a*’. The fixed conductance causality of the switch resistors leads to a causal conflict at the 0-junctions representing the potential of the nodes between upper and lower switches in a half-bridge. These causal conflicts are resolved by adding an auxiliary C-storage element to these 0-junctions. Equations are derived from the BG in such a way that their capacitances can be set to zero. Consequently, the small ON-resistance of the switches and the small node capacitances do not lead to small time constants.

Fault scenarios within the power inverter

This article uses this BG model for the study of some fault scenarios within the power inverter. Under normal operation, the two switches in one leg commute complementarily. That is, if one switch is on, the other one is off. Due to non-proper functioning of the switches, 2^6 theoretical switch state combinations may be possible. In Welchko et al.,¹⁸ the authors consider fault tolerant inverter topologies used for an alternating current (AC) motor drive. In their article, they list the following faults within the power inverter.

1. Single inverter switch short circuit (the lower switch in a leg is permanently on).

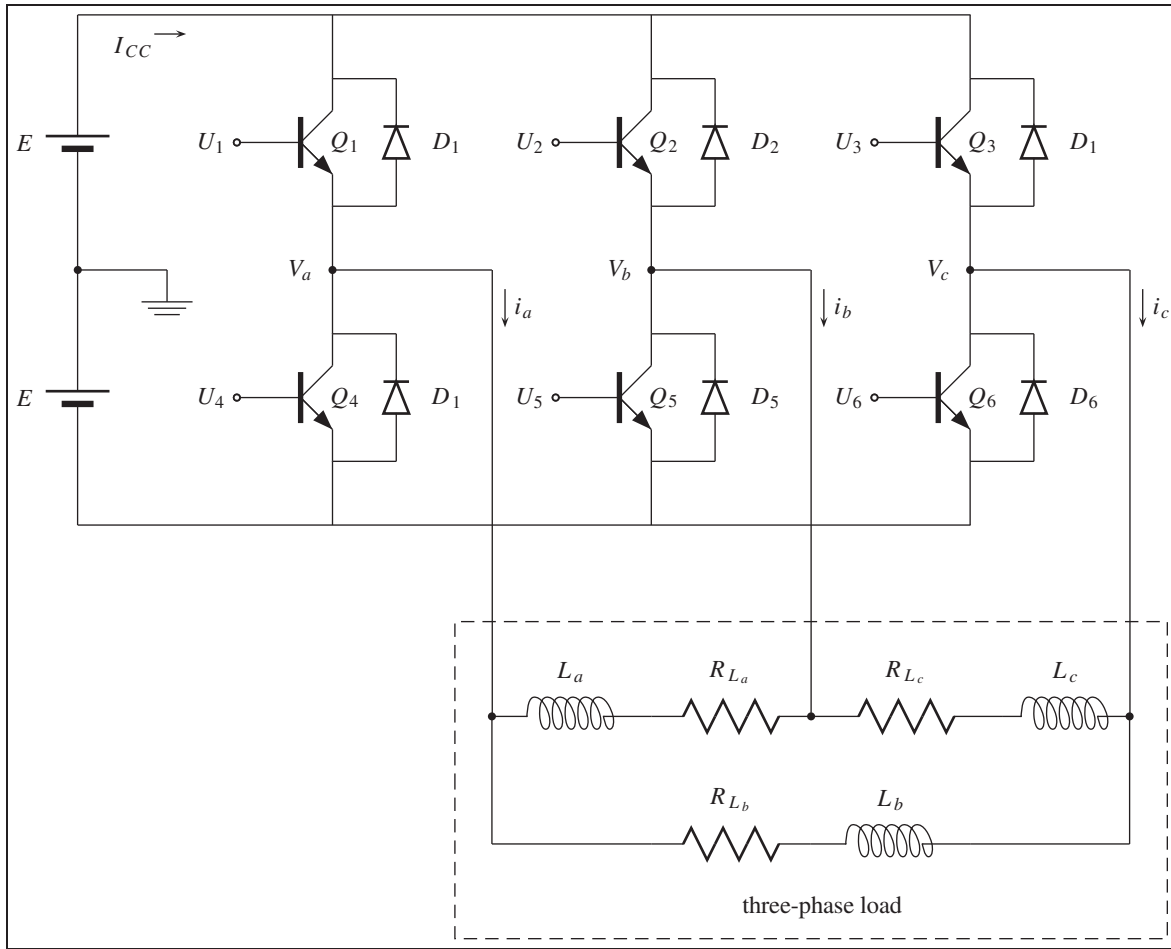


Figure 3. Circuit schematic of a switched three-phase power inverter.

2. Phase-leg short circuit (both switches in a leg are permanently on).
3. Single inverter switch open circuit (one switch in a leg is permanently off).
4. Single-phase open circuit (both switches in a leg commute complementarily, but the phase line between the half-bridge and the AC motor is permanently disrupted).

In the following, these fault scenarios are analysed. The presentation is confined to the consideration of faults in leg ‘a’. The same considerations apply to the other two legs.

The BG model of the upper switch of half-bridge ‘a’ (Figure 5) yields for the current i_{a_p} through the switch

$$i_{a_p} = \frac{m_{a_p}^2}{R_{a_p}}(E - V_a) \tag{1}$$

Likewise, the current i_{a_n} through the lower switch of half-bridge ‘a’ reads

$$i_{a_n} = \frac{m_{a_n}^2}{R_{a_n}}(E - V_a) \tag{2}$$

Summation of flows at the 0-junction for V_a in Figure 4 gives

$$C_a \dot{V}_a = i_{a_p} + i_{a_n} - i_a = \frac{m_{a_p}^2}{R_{a_p}}(E - V_a) + \frac{m_{a_n}^2}{R_{a_n}}(E - V_a) - i_a \tag{3}$$

Let $C_a \rightarrow 0$. Then, equation (3) becomes an algebraic equation that can be solved for V_a . Observing $m_{a_p}^2(t) = m_{a_p}(t) \in \{0, 1\}$, $m_{a_n}^2(t) = m_{a_n}(t) \in \{0, 1\}$ and assuming $R_{a_n} = R_{a_p} = R_a$, the result is

$$V_a = \frac{m_{a_p} - m_{a_n}}{m_{a_p} + m_{a_n}} E - \frac{R_a}{m_{a_p} + m_{a_n}} i_a \tag{4}$$

Healthy inverter. In case both switches commute complementarily $m_{a_n} = 1 - m_{a_p}$, that is, in a healthy power inverter, the equation for the potential V_a reads

$$V_a = (2m_{a_p} - 1)E - R_a i_a \tag{5}$$

As the ON-resistance R_a of the switches in leg ‘a’ is rather small, the second term in equation (5) may become negligible, which means that V_a basically switches between $+E$ and $-E$ as to be expected.

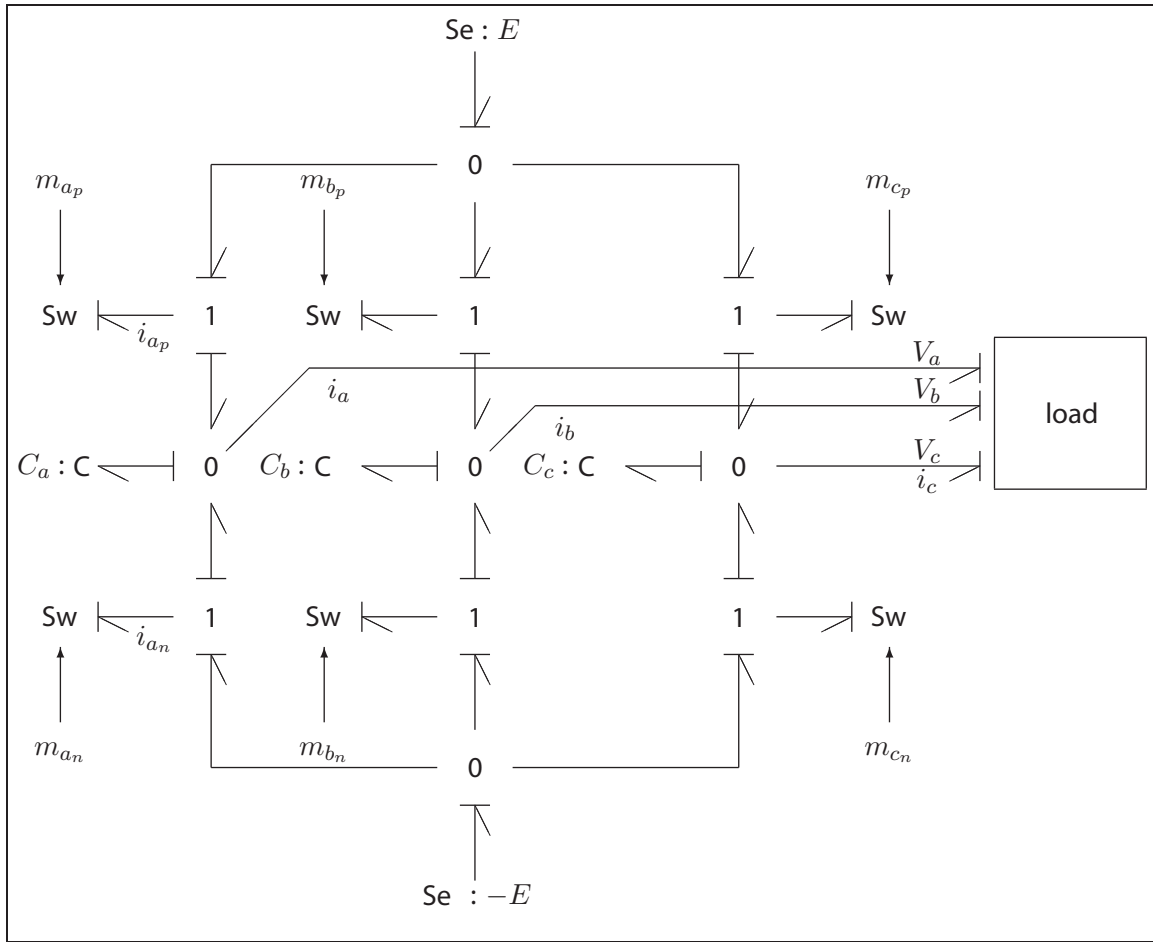


Figure 4. Bond graph of the switched three-phase power inverter.

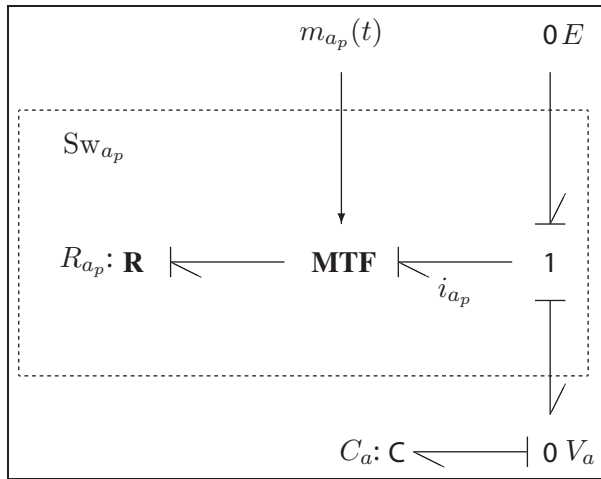


Figure 5. Bond graph model Sw of a switch considered non-ideal illustrated for the upper switch in half-bridge 'a'.

Case 1. The lower switch in leg 'a' is permanently on

The case of a single inverter switch short circuit, in which the lower switch is permanently on, can be captured by letting $m_{a_n} = \tilde{m}_{a_n} = 1$. As a result

$$V_a = \frac{m_{a_p}}{m_{a_p} + 1} E - \frac{R_a}{m_{a_p} + 1} i_a \tag{6}$$

Case 2. Both switches in leg 'a' are permanently on

In case of a phase-leg short circuit, in which both switches in leg 'a' are permanently on, V_a becomes

$$V_a = \frac{R_a}{2} i_a \tag{7}$$

Case 3. The lower switch in leg 'a' is permanently off

Clearly, in case of a single inverter switch open circuit, fault (4) is not applicable. If one switch is permanently off, then $m_{a_p} = m_{a_n} = 0$ during the time intervals in which the other still operating switch is also off. Suppose that the lower switch is permanently off and while the upper one is functioning. Then

$$V_a = E + R_a i_a \tag{8}$$

when the upper switch is on. During this time interval, this case is identical with the one in which both switches commute complementarily. However, when the upper

switch Sw_{ap} is off, then the node with the potential V_a is not connected to the node supplying the voltage $+E$. As its capacitance C_a to ground is neglected, there is no current i_a on phase line 'a' and $V_a = E$. That is, V_a does not switch between values $+E$ and $-E$ but retains the value $+E$. Furthermore, if the delta network of the RL -load is converted into a BG, then causality assignment results in integral causality for the I -elements of all inductors. However, $i_a = 0$ periodically for a time interval means that two inductor currents must be equal, that is, one I -element becomes dependent temporarily.

Bond graph model of the RL -load

Integral causality can be kept for the three I -elements in the model of the RL -load regardless of the state of switch Sw_{ap} by adding a residual effort sink as proposed in equation (15) and as shown in Figure 6. The artificial effort sink enforces that the two inductor currents i_{L_a} and i_{L_c} become equal when switch Sw_{ap} is off and thus accounts for the temporary decrease of the number of state variables. The moduli of the transformers in the BG of Figure 6 enable to adapt the model to various fault situations. In normal operation, one of the two switches in leg 'a' is on, while the other one is off. In this case, $b_1 = 1$ and $b_2 = b_3 = b_4 = b_5 = b_6 = 0$.

1. The lower switch in leg 'a' is permanently on: $b_1 = 1$ and $b_2 = b_3 = b_4 = b_5 = b_6 = 0$.
2. Both switches in leg 'a' are permanently on: $b_1 = 1$ and $b_2 = b_3 = b_4 = b_5 = b_6 = 0$.

3. The lower switch in leg 'a' is permanently off: $b_1 = 0, b_2 = 1, b_3 = 0, b_4 = 1, m_{ap}$ and $b_5 = b_6 = 0$.
4. Both switches in leg 'a' commute complementarily, but line 'a' to the load is permanently disrupted: $b_1 = 0, b_2 = b_3 = 0$ and $b_4 = b_5 = b_6 = 1$.

Case 3. The lower switch in leg 'a' is permanently off

The effort necessary to temporarily enforce that $i_{L_a} = i_{L_c}$ when both switches in leg 'a' are off can be deduced by summing efforts at 1-junctions 1_1 and 1_2

$$E - V_b - R_{L_a}i_{L_a} - \lambda = V_c - E - R_{L_c}i_{L_c} + \lambda \quad (9)$$

Hence

$$\lambda = E - \frac{1}{2}(V_b + V_c) \quad (10)$$

In case the lower switch in leg 'a' is permanently off while the upper one is functioning, then the currents i_{L_a} and i_{L_c} jump to a common value i_s when the upper switch opens so that $i_a = 0$. Let t_o denote the time instant of such a switching event and δ the magnitude of the jump. Then

$$i_{L_a}(t_o) + \delta = i_{L_c}(t_o) \quad \delta = i_s \quad (11)$$

Thus

$$\delta = \frac{1}{2}[i_{L_c}(t_o) - i_{L_a}(t_o)] \quad (12)$$

This jump at time instances t_o means that the numerical integration of the model equations must be re-initialised at t_o . When the upper switch abruptly closes at time instances t_c , then both currents i_{L_a} and i_{L_c} start from their common value.

Case 4. Both switches commute, but line 'a' is permanently disrupted

In this case, the inductor currents i_{L_a} and i_{L_c} are permanently equal. Accordingly, the residual sink must be switched on permanently, that is, $b_4 = 1$, while the other transformer moduli vanish. The potential V is unknown. However, summation of efforts at 1-junctions 1_1 and 1_2 yields the following

$$0 = V - R_{L_a}i_{L_a} - L_a \frac{d}{dt}i_{L_a} - V_b - \lambda \quad (13)$$

$$0 = V_c - R_{L_c}i_{L_c} - L_c \frac{d}{dt}i_{L_c} - V + \lambda \quad (14)$$

It is assumed that $R_{L_a} = R_{L_c}$ and $L_a = L_c$. Then, the equality of the two inductor currents i_{L_a} and i_{L_c} enforced by the residual effort sink gives

$$V - \lambda = \frac{1}{2}(V_b + V_c) \quad (15)$$

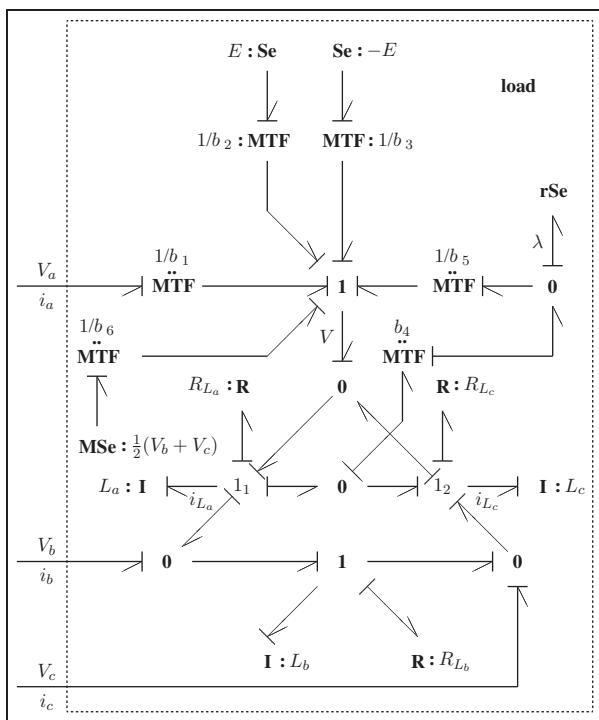


Figure 6. Bond graph of the three-phase RL -load in delta configuration accounting for a temporary decrease of states.

It is this difference that is needed to compute the right-hand side of the ODEs for the inductor currents i_{L_a} and i_{L_c} .

Equations of the RL-load accounting for all modes. It is straightforward to derive the equations for the RL-load from the BG in Figure 6

$$V = b_1 V_a + b_2 E \quad b_3 E + b_5 \lambda + b_6 \frac{1}{2}(V_b + V_c) \quad (16)$$

$$\frac{d}{dt} i_{L_a} = \frac{1}{L_a} [V \quad R_{L_a} i_{L_a} \quad V_b \quad b_4 \lambda] \quad (17) \leftarrow$$

$$\frac{d}{dt} i_{L_b} = \frac{1}{L_b} [V_b \quad R_{L_b} i_{L_b} \quad V_c] \quad (18) \leftarrow$$

$$\frac{d}{dt} i_{L_c} = \frac{1}{L_c} [V_c \quad R_{L_c} i_{L_c} \quad V + b_4 \lambda] \quad (19) \leftarrow$$

$$i_a = i_{L_a} \quad i_{L_c} \quad (20) \leftarrow$$

$$i_b = i_{L_b} \quad i_{L_a} \quad (21) \leftarrow$$

$$i_c = i_{L_c} \quad i_{L_b} \quad (22) \leftarrow$$

Simulation results

The equations derived from the BG of the power inverter connected to a delta RL-load have been implemented in the Scilab script language.¹⁹ The above-considered fault scenarios have been simulated. In the following, some of the results are presented. Faulty variables are discriminated from their counterparts in the healthy system by a tilde. In subsequent figures displaying simulation results, the tilde is expressed by prefixing a variable name by the letter *t*, for example, $\tilde{i}_{L_a} = t i_{L_a}$.

Fault scenario 1: the lower switch in leg ‘a’ is permanently on. In this case, the mathematical model to be solved is simply a set of three linear ODEs for the three inductor currents being the state variables. Figure 7 shows that the permanently closure of the lower switch leads to reduced values of the current i_a when the upper switch is on ($m_{a_p} = 1$). Figure 8 displays the time history of the load currents i_{L_c} and \tilde{i}_{L_c} . The load current i_{L_b} is not affected by this fault. However, the load current i_{L_c} is affected and because of the nodicity property of the delta network

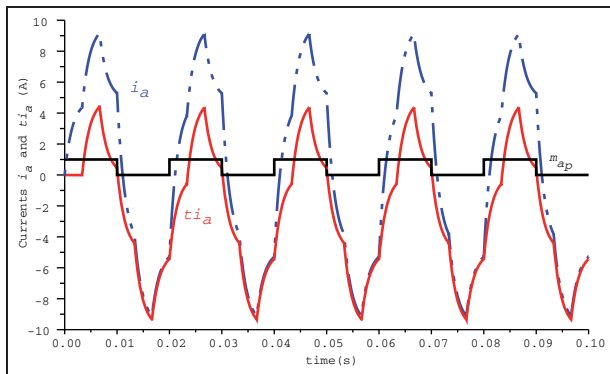


Figure 7. Currents i_a and \tilde{i}_a in case the lower switch S_{a_n} is permanently on.

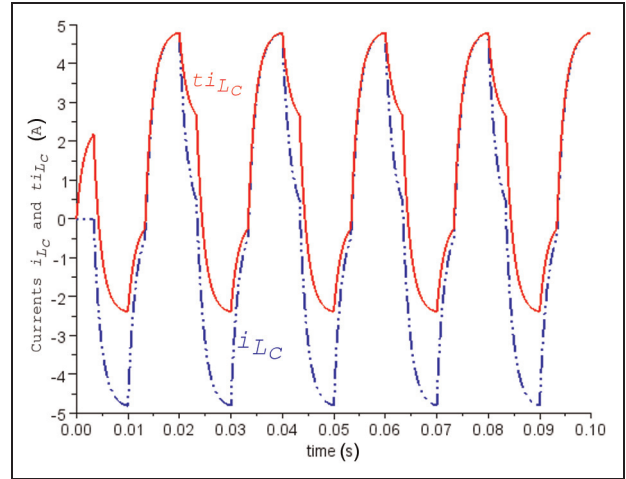


Figure 8. Load currents i_{L_c} and \tilde{i}_{L_c} in case the lower switch S_{a_n} is permanently on.

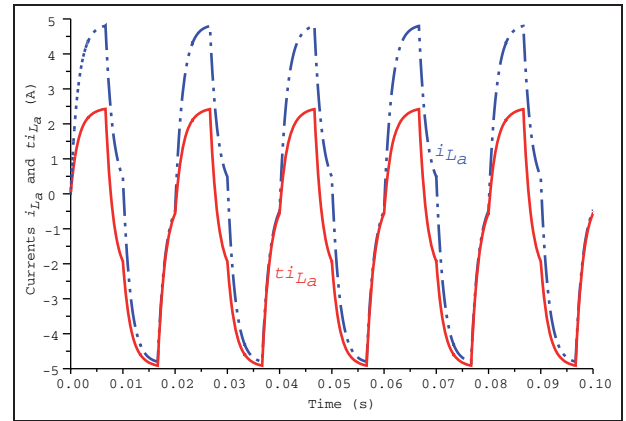


Figure 9. Load currents i_{L_a} and \tilde{i}_{L_a} in case the lower switch S_{a_n} is permanently on.

$$i_{L_a} + i_{L_b} + i_{L_c} = 0 \quad (23) \leftarrow$$

not directly displayed by the BG of the RL-load, the remaining load current i_{L_a} must also be affected as shown in Figure 9.

Fault scenario 3: the lower switch in leg ‘a’ is permanently off. In this case, line ‘a’ is disconnected from the voltage supply $+E$ when the upper switch S_{a_p} is off, that is, the current on line ‘a’ vanishes, $\tilde{i}_a = 0$. Consequently, the two load currents \tilde{i}_{L_a} and \tilde{i}_{L_c} must be equal. While keeping integral causality at the two *I*-elements $I : L_a$ and $I : L_c$ providing these currents, their equality is enforced by the residual effort sink $rSe : \lambda$. Accordingly, Figure 10 shows that, in this case, $\tilde{i}_a = 0$ when $m_{a_p} = 0$. Figure 11 clearly shows that the two load currents \tilde{i}_{L_a} and \tilde{i}_{L_c} jump to a joint value whenever the upper switch S_{a_p} opens. As long as the switch is open, both currents are equal so that $\tilde{i}_a = 0$.

Figure 11 shows that the jump happens at $t_0 = T/2 = 0.01s$ and that $\tilde{i}_{L_a} \approx 0.5A$ and $\tilde{i}_{L_c} \approx 4.8A$.

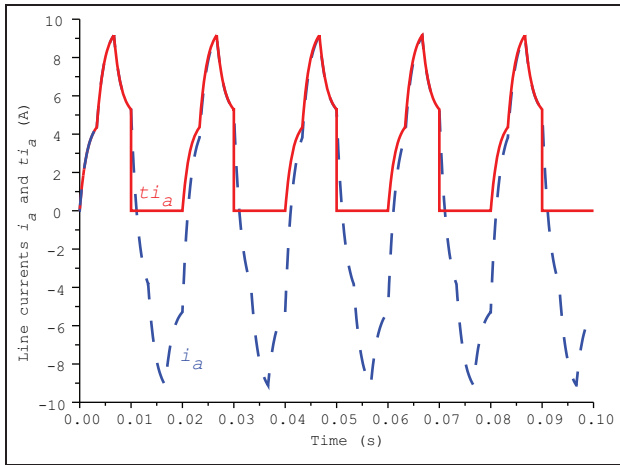


Figure 10. Line currents i_a and \tilde{i}_a in case the lower switch S_{a_n} is permanently off.

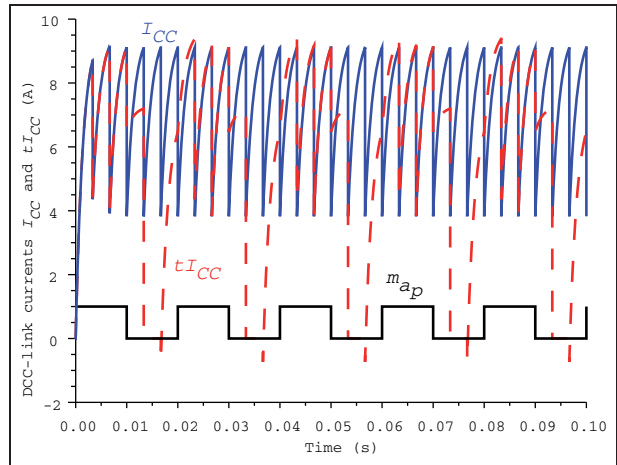


Figure 12. DCC-link currents I_{CC} and \tilde{I}_{CC} in case the lower switch S_{a_n} is permanently off.

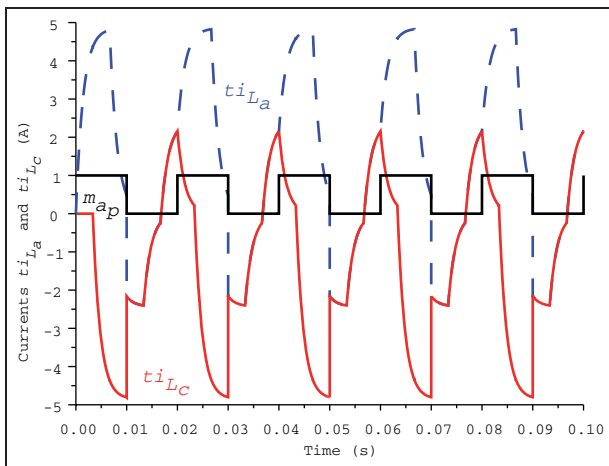


Figure 11. Load currents \tilde{i}_{L_a} and \tilde{i}_{L_c} in case the lower switch S_{a_n} is permanently off.

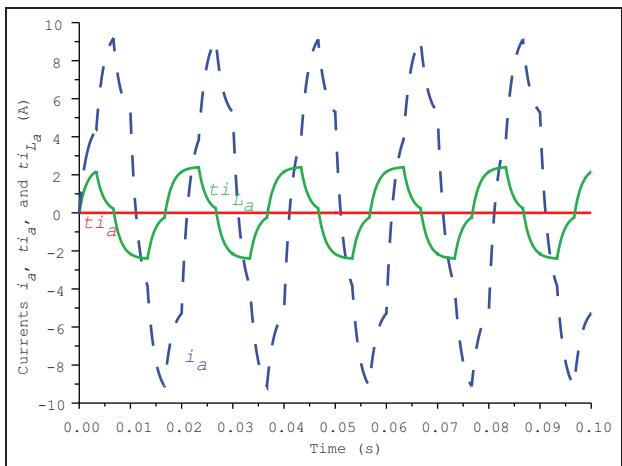


Figure 13. Currents i_a , \tilde{i}_a and \tilde{i}_{L_a} in case line 'a' is disrupted.

According to equation (12), $\delta = (4.8 - 0.5)/2 = 2.65\text{A}$. Hence, the joint value of the two currents at t_0 is $i_s = \tilde{i}_{L_a} + \delta = 2.65 + 0.5 = 2.15\text{A}$ in agreement with Figure 11.

Clearly, a permanently open lower switch S_{a_n} also affects the direct current (DC)-link current I_{CC} .

$$\begin{aligned} \tilde{I}_{CC} &= \tilde{i}_{a_p} + \tilde{i}_{b_p} + \tilde{i}_{c_p} \\ &= m_{a_p} \tilde{i}_a + m_{b_p} \tilde{i}_b + m_{c_p} \tilde{i}_c \end{aligned} \quad (24) \leftarrow$$

The current through one of the upper switches is different from zero only if the switch is on. In the healthy inverter, the lower switch then is off, that is, the current through an upper switch equals the current on the line connecting the half-bridge to the load. In the fault scenario under consideration, the lower switch $S_{w_{a_n}}$ is permanently off. As can be seen from Figure 12, the disturbed DC-link current \tilde{I}_{CC} deviates from the non-faulty one, I_{CC} , during those time intervals in which the upper switch is off ($m_{a_p} = 0$), that is, when leg 'a' does not contribute any current.

Fault scenario 4: both switches commute complementarily, line 'a' is disrupted from the load. At $t = 0$, the upper switch $S_{w_{a_p}}$ is closed. It is assumed that line 'a' is permanently disrupted shortly afterwards, that is, $i_a = 0$ for $t > 0$. This means that the residual effort source $rSe : \lambda$ must permanently enforce $i_{L_a} = i_{L_c}$. Furthermore, though the switches in leg 'a' commute, there is no connection of this leg to the load. Hence

$$\begin{aligned} \tilde{I}_{CC} &= \tilde{i}_{a_p} + \tilde{i}_{b_p} + \tilde{i}_{c_p} \\ &= m_{a_p} \times 0 + m_{b_p} \tilde{i}_b + m_{c_p} \tilde{i}_c \end{aligned} \quad (25) \leftarrow$$

Accordingly, Figure 13 displays the time evolution of the currents i_a , \tilde{i}_a and \tilde{i}_{L_a} . Figure 14 depicts the DC-link currents I_{CC} and \tilde{I}_{CC} . As the current \tilde{i}_a on line 'a' is permanently zero, the time evolution of the disturbed DC-link current \tilde{I}_{CC} clearly differs from the one in the previous case in which leg 'a' is temporarily disconnected from the load whenever the upper switch $S_{w_{a_p}}$ is off (Figure 12).

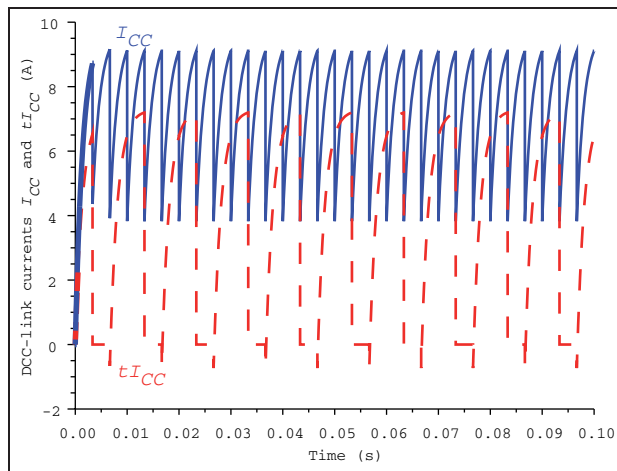


Figure 14. DCC-link currents I_{CC} and \tilde{I}_{CC} in case line 'a' is disrupted.

Fault indicators

The previous sections consider some fault scenarios within the power inverter. Simulation runs show their effect on the RL -load. For the supervision of a real system, it is of fundamental importance to conclude from data taken by sensors whether a fault has happened and to locate the malfunctioning.

Analytical redundancy relations. As to a BG model-based approach to FDI, it is well known that fault detections can be obtained from balances of power variables at junctions. If the constitutive equations of elements in a BG model permit to eliminate unknown variables from the balance of power variables at a junction, then the result is a constraint between known input and measured output variables known as analytical redundancy relation (ARR). Numerical evaluation of an ARR produces a value termed residual. Ideally, it is equal to zero at any time instant. However, input disturbances, measurement noise, parameter uncertainties and numerical inaccuracies may lead to values different from zero. As long as they are within certain bounds, no fault has happened. In other words, if values significantly exceeds given thresholds in a time interval, then this is an indication that a fault has happened, that is, ARR residuals can serve as fault indicators. For hybrid systems, the dynamic behaviour in one system mode may be very different from the one in another mode. Therefore, it is important to determine system mode-dependent thresholds in order to avoid false fault alarms or to avoid missing true faults.¹³

Fault signature matrices. If unknowns in the balances of power variables at junctions can be eliminated, then the information which system component contributes to which ARR is usually captured in a structural fault signature matrix (FSM) with rows indicating components and columns indicating ARRs. If the i th component

contributes to the j th ARR, then this is indicated by a matrix entry '1' at position (i, j) , if not by '0'. From the structure of such a binary FSM, it can be deduced whether a fault can be detected and, moreover, whether it can be isolated (see, for instance, Borutzky² and Samantaray and Ould Bouamama²⁰). The structural information presented in an FSM can also be obtained directly from a causal diagnostic bond graph (DBG) by following causal paths from known inputs to virtual detectors of ARR residuals.²⁰ Moreover, software such as SYMBOLS²¹ or Model Builder²² can automatically generate ARRs in a symbolic form.

Numerical computation of ARRs. An advantage of a BG model-based approach to FDI is that numerical model computation can produce the time evolution of such residuals even when unknowns cannot be eliminated analytically.^{1,23,24} One way to numerically compute the residuals is to feed measured variables from a real process (online simulation) or provided by computation of a behavioural model of the real process (offline simulation) into a DBG with storage elements in preferred derivative causality and virtual detectors for the residuals.²³ Another approach proposed by the author is to couple a behavioural BG model of the process subject to faults to a BG of the non-faulty process by means of residual sinks. Their input is the difference of the power variables of corresponding junctions in the two BGs. Their output is such that the difference becomes zero and is imposed on the junction in the BG of the non-faulty system. As a result, the non-faulty system adapts its behaviour to one of the faulty systems. The outputs of the residual sinks coupling the two models are just the residuals to be determined.^{1,24} In the following, the latter approach is used for computing the residuals in two of the above-considered fault scenarios.

Fault scenario 4. Both switches commute complementarily, line 'a' is disrupted from the load

The disruption of line 'a' is assumed to happen at time instant t_1 , that is, the current \tilde{i}_a vanishes for $t \geq t_1$. In order to ensure that the two inductor currents \tilde{i}_{L_a} and \tilde{i}_{L_c} are equal for $t > t_1$, the residual effort sink in the BG model of the RL -load must be activated at $t = t_1$. This system mode change is achieved by appropriately choosing the transformer moduli. Let $\text{step}(t, t_1)$ denote the unit-step function with a jump from zero to one at $t = t_1$. Then, $b_1 = 1 - \text{step}(t, t_1)$, $b_2 = \text{step}(t, t_1)$, $b_3 = 0$ and $b_4 = \text{step}(t, t_1)$. Hence, the models of the faulty and the non-faulty systems are quite different for $t \geq t_1$.

It is assumed that the currents $\tilde{i} = \tilde{I}_{CC}$ through the voltage source $\text{Se}: +E$, the current \tilde{i}_a on line 'a' and the inductor current \tilde{i}_{L_a} have been 'measured'. As can be seen from Figure 15, the BGs of the faulty system and the non-faulty one are coupled by a residual effort

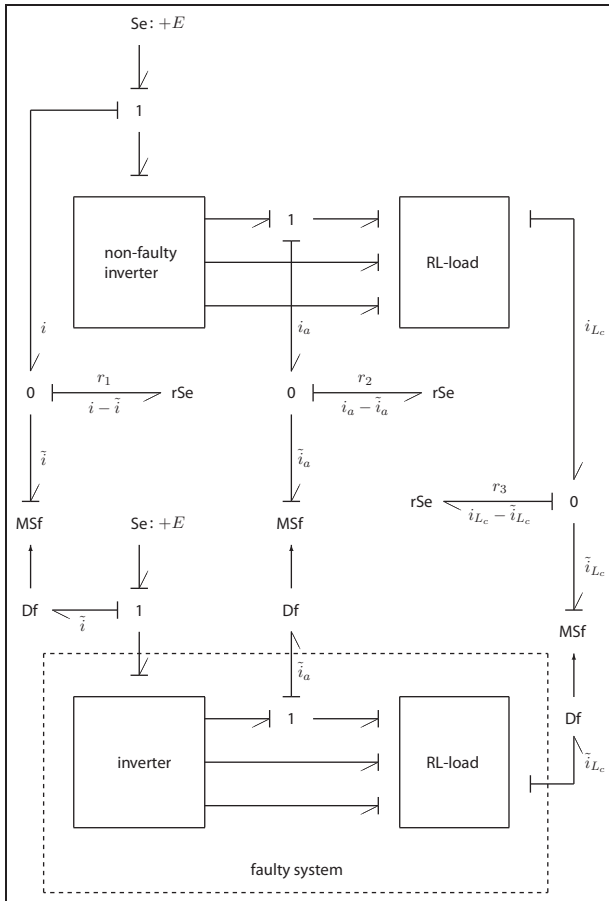


Figure 15. Coupling of a bond graph of the faulty system (lower part) to a bond graph of the non-faulty system (upper part) by means of residual effort sinks.

sink that enforces $i_a = \tilde{i}_a$. Another residual effort sink ensures that $i_{Lc} = \tilde{i}_{Lc}$. A third residual effort sink is used to adapt the DC-link current I_{CC} .

The mathematical model that can be derived from the coupled BGs is clearly a DAE system. Approximating the function of the coupling residual effort sinks by a pair of an artificial C element and an artificial resistor results in an ODE system. The following results of a Scilab simulation run clearly show that due to the coupling of the two models, the non-faulty system indeed adapts its behaviour to the faulty one for $t \geq t_1 = 0.05$ s (Figures 16–18). Accordingly, this system mode change is reflected by the time evolution of the residuals (Figures 19–21). Besides the finite Dirac pulses at switching times, the values of the residuals are clearly out of any small bounds indicating that a fault has happened for $t \geq t_1$.

Fault scenario 2. Both switches in leg ‘a’ are permanently on

In this case, lines a , b and c permanently connect the power inverter to the RL -load. The three I -storage elements of the load model are independent, so that the residual effort sink in the load model is not needed.

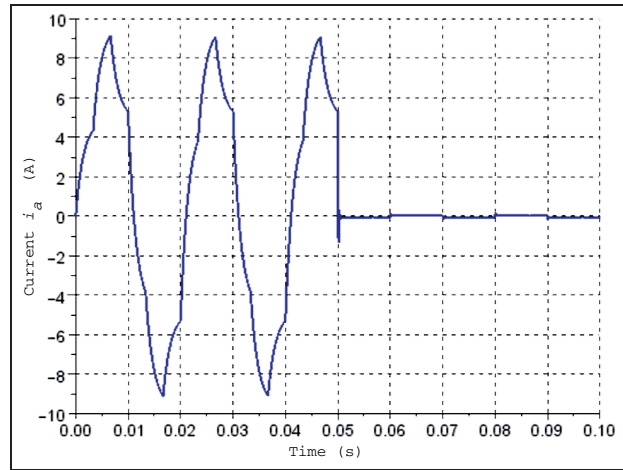


Figure 16. Line current i_a in case line ‘a’ is disrupted for $t > 0.05$ s.

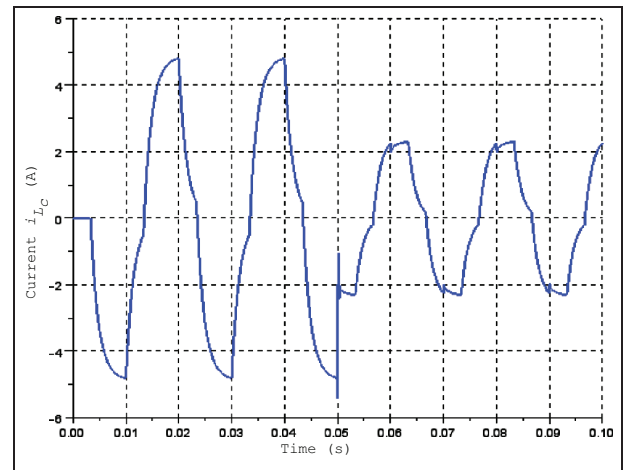


Figure 17. Inductor current i_{Lc} in case line ‘a’ is disrupted for $t > 0.05$ s.

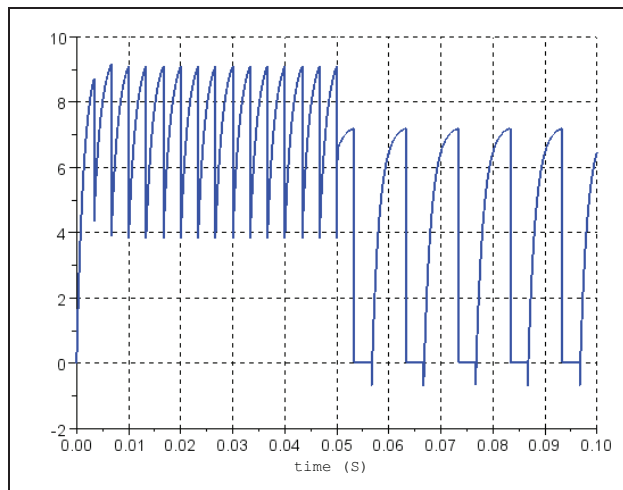


Figure 18. DC-link current I_{CC} in case line ‘a’ is disrupted for $t > 0.05$ s.

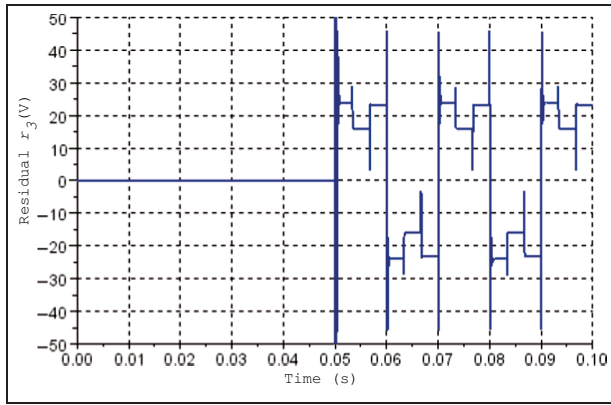


Figure 19. Residual r_3 in case line 'a' is disrupted for $t > 0.05$ s.

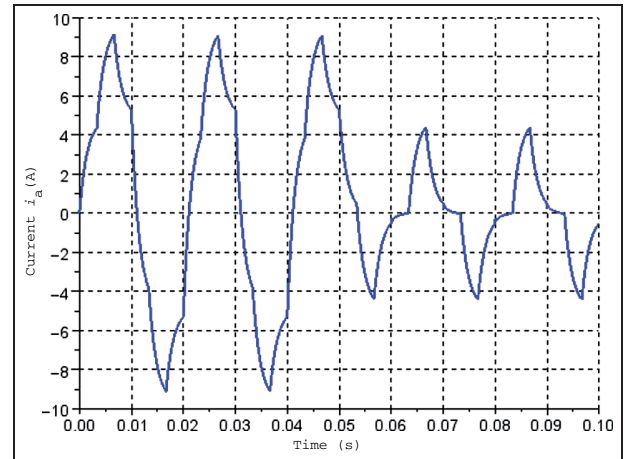


Figure 22. Current i_a on line 'a' in case both switches in leg 'a' are permanently on for $t > 0.05$ s.

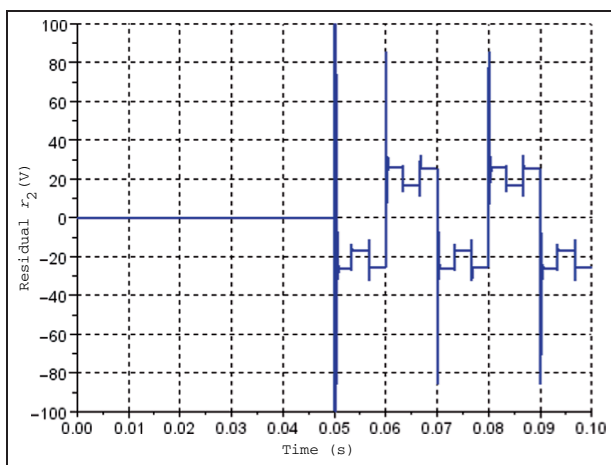


Figure 20. Residual r_2 in case line 'a' is disrupted for $t > 0.05$ s.

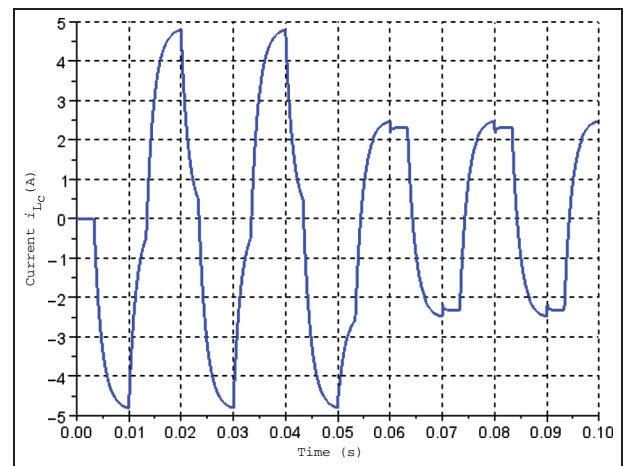


Figure 23. Inductor current i_{L_c} in case both switches in leg 'a' are permanently on for $t > 0.05$ s.

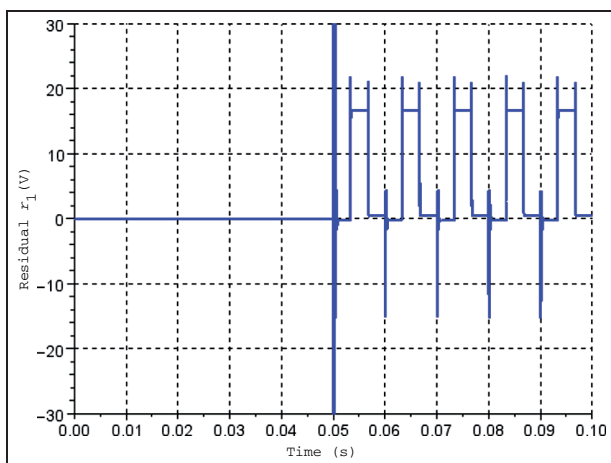


Figure 21. Residual r_1 in case line 'a' is disrupted for $t > 0.05$ s.

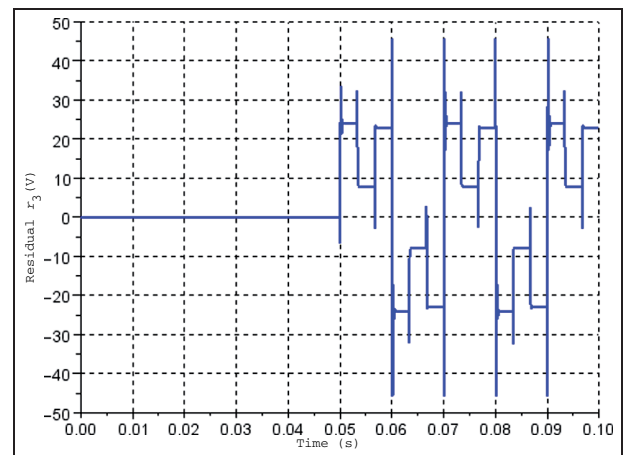


Figure 24. Residual r_3 in case both switches in leg 'a' are permanently on for $t > 0.05$ s.

The switches in leg 'a' are permanently on affecting the potential V_a according to equation (7), which in turn has an impact on the inductor currents i_{L_a} and i_{L_c} . This is confirmed by the simulation results depicted in Figures 22 and 23. Figures 26, 25, 24 show the time evolution of the residuals r_1 , r_2 and r_3 enforcing that

the healthy system model adapts its behaviour to the faulty one.

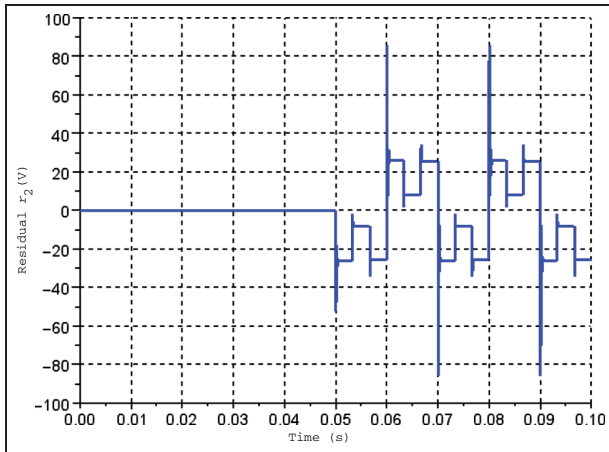


Figure 25. Residual r_2 in case both switches in leg 'a' are permanently on for $t > 0.05$ s.

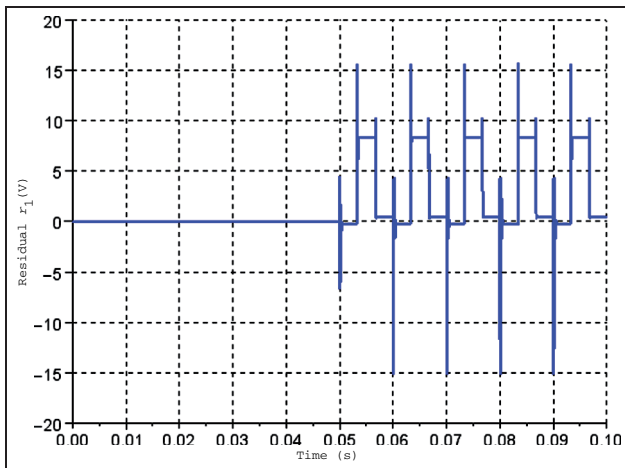


Figure 26. Residual r_1 in case both switches in leg 'a' are permanently on for $t > 0.05$ s.

Conclusion

This article shows that the modelling of switching devices by means of a transformer–resistor pair can well be combined with the use of residual sinks in an approach to BG model–based FDI of switched power electronic systems that has the following features:

- one single BG for all system modes;
- no non-standard BG elements;
- application of the unmodified standard SCAP;
- time-invariant preferred integral causality;
- one set of ARRs for all system modes.

In case the outputs of residual sinks cannot analytically be determined, they can be computed numerically as components of the descriptor vector of a DAE system. The simulation of fault scenarios requires a numerical solver with the capability of resetting the integration at switching times.

The study of faults in a three-phase switching power inverter in this article can be extended by considering

further fault situations not addressed due to the lack of space. Furthermore, the study may be continued by replacing the model of the RL -load by a model of an AC motor. The power inverter is a standard subsystem of practical relevance, but the presented approach is not confined to power electronic systems and can be used for hybrid systems in other domains as well.

Transformers with 'Boolean' modulus accounting for system mode changes used in this approach, or ideal switches or controlled junctions in other approaches, temporarily disconnect and reconnect causal paths between elements. Therefore, continuation of this work will also address structural controllability and structural observability in hybrid systems.

Funding

This research received no specific grant from any funding agency in the public, commercial or not-for-profit sectors.

Acknowledgement

The case study of the switched three-phase power inverter was inspired by discussions with Prof. S. Junco and his PhD student M. Nacusse on fault tolerant control and model-based fault detection and isolation during the author's stay at the Universidad Nacional de Rosario (UNR), Argentina.

References

1. Borutzky W. Bond-graph-based fault detection and isolation for hybrid system models. *Proc IMechE, Part I: J Systems and Control Engineering* 2012; 226: 742–760.
2. Borutzky W. *Bond graph methodology – development and analysis of multidisciplinary dynamic system models*. London: Springer-Verlag, 2010.
3. Garcia-Gomez J. *Approche bond graph pour la modélisation des effets thermiques dans les composants de commutation en électronique de puissance*. PhD Thesis, Université des Sciences et Technologies de Lille, France, 1997.
4. Ducreux JP, Dauphin-Tanguy G and Rombaut C. Bond graph modelling of commutation phenomena in power electronic circuits. In: *International conference on bond graph modeling (ICBGM'93): proceedings of the 1993 western simulation multiconference* (eds JJ Granda and FE Cellier), La Jolla, CA, USA, 17–20 January 1993, Simulation Series, vol. 25, no. 2, pp.132–136. SCS Publishing.
5. Dauphin-Tanguy G and Rombaut C. Why a unique causality in the elementary commutation cell bond graph model of a power electronics converter. *IEEE Int Conf Sys, Man and Cybernetics* 1993; 1: 257–263.
6. Umarikar AC. *Modelling of switched mode power converters: a bond graph approach*. PhD Thesis, Centre for Electronics Design and Technology, Indian Institute of Science, India, 2006.
7. Buisson J, Cormerais H and Richard P-Y. Analysis of the bond graph model of hybrid physical systems with ideal switches. *Proc IMechE, Part I: J Systems and Control Engineering* 2002; 216(1): 47–63.

8. Edstrom K. *Switched bond graphs: simulation and analysis*. PhD Thesis, Linköping University, Sweden, 1999.
9. Stromberg JE. *A mode switching modelling philosophy*. PhD Thesis, Linköping University, Sweden, 1994.
10. Asher GM. The robust modelling of variable topology circuits using bond graphs. In: *International conference on bond graph modeling (ICBGM'93): proceedings of the 1993 western simulation multiconference* (eds JJ Granda and FE Cellier), La Jolla, CA, USA, 17–20 January 1993, Simulation Series, vol. 25, no. 2, pp.126–131. SCS Publishing.
11. Roychoudhury I, Daigle M, Biswas G, et al. A method for efficient simulation of hybrid bond graphs. In: *Proceedings of the international conference on bond graph modeling and simulation* (eds JJ Granda and FE Cellier), 11–14 January 2007, vol. 39, no. 1, pp.177–184. San Diego, CA, USA: SCS Publishing.
12. Mosterman PJ. *Hybrid dynamic systems: a hybrid bond graph modeling paradigm and its application in diagnosis*. PhD Thesis, Vanderbilt University, USA, 1997.
13. Borutzky W. Fault indicators and adaptive thresholds from hybrid system models. In *7th Vienna international conference on mathematical modelling*, Vienna, Austria, 14–17 February 2012.
14. Borutzky W (ed). *Bond graph modelling of engineering systems – theory, applications and software support*. New York: Springer-Verlag, 2011.
15. Borutzky W. Representing discontinuities by means of sinks of fixed causality. In: *International conference on bond graph modeling (ICBGM'95): proceedings of the 1995 western simulation multiconference* (eds FE Cellier and JJ Granda), Las Vegas, Nevada, USA, 15–18 January 1995, Simulation Series, vol. 27, no. 1, pp.65–72. SCS Publishing.
16. Junco S, Diguez G and Ramirez F. On commutation modeling in bond graphs. In: *Proceedings of the international conference on bond graph modeling (ICBGM 2007)* (eds JJ Granda and F Cellier), San Diego, CA, USA, 2007, Simulation Series, vol. 39, no. 1, pp.12–19. SCS Publishing.
17. Controllab Products. 20-sim the power in modeling, <http://www.20sim.com>
18. Welchko BA, Lipo TA, Jahns TM, et al. Fault tolerant three-phase AC motor drive topologies: a comparison of features, costs, and limitations. *IEEE Trans Power Electronics* 2004; 19(4): 1108–1116.
19. Scilab Consortium. Scilab, <http://www.scilab.org/>
20. Samantaray AK and Ould Bouamama B. *Model-based process supervision – a bond graph approach*. *Advances in industrial control*. London: Springer, 2008.
21. HighTec Consultants. SYMBOLS Sonata, <http://www.htcinfo.com/>
22. Ould Bouamama B, Samantaray AK, Medjaher K, et al. Model builder using functional and bond graph tools for FDI design. *Control Engng Pract* 2005; 13(7): 875–891.
23. Samantaray AK, Medjaher K, Ould Bouamama B, et al. Diagnostic bond graphs for online fault detection and isolation. *Simulation Modelling Practice and Theory* 2006; 14(3): 237–262.
24. Borutzky W. Bond graph model-based fault detection using residual sinks. *Proc IMechE, Part I: J Systems and Control Engineering* 2009; 223(3): 337–352.

Appendix I

Notation

a, b, c	indices
C	capacitance
D	diode
D_f	flow detector
E	voltage supply
L	self-inductance
$m(t)$	transformer modulus $m(t) \in \{0, 1\}$
$m_{ap}(t)$	transformer modulus of the upper switch of the half-bridge with the index a
n	index indicating the lower switch of a half-bridge
p	index indicating the upper switch of a half-bridge
Q_i	transistor i of the power inverter
r_i	residual i
R	resistance
R_{on}	resistance of a switch in ON-mode
rSe	residual effort sink
Sw	switch
Sw_{ap}	upper switch in the half-bridge with the index a
t	time
$U_i(t)$	control voltage at the base of transistor Q_i
V	voltage
λ	output of a residual effort sink

Parameters of the switched three-phase power inverter with RL-load

```
// Control signals
omega = 314.159; // [rad/s] = 2*pi/T; T = 0.02 [s]
phase1 = 0.0;
phase2 = 4.1888; // = 240°
phase3 = 2.0944; // = 120°
maximum = 1.0;
minimum = 0.0;

// Voltage supply
E = 25; // [V]

// Delta RL-load:
RLa = 10; // [Ohm]
RLb = RLa;
RLc = RLa;

La = 0.015; // [H]
Lb = La;
```